PHYSICAL REVIEW B **104**, L081102 (2021)

Letter

Enhanced lattice fluctuations prior to a nonmagnetic ferroelectric order in an ionic spin-chain system

Keishi Sunami,[1,*] Tomohiro Baba,[1] Kazuya Miyagawa,[1] Sachio Horiuchi,[2] and Kazushi Kanoda[1,†]
[1]*Department of Applied Physics, University of Tokyo, Bunkyo-ku, Tokyo 113-8656, Japan*
[2]*Research Institute for Advanced Electronics and Photonics (RIAEP), National Institute of Advanced Industrial Science and Technology (AIST), Tsukuba, Ibaraki 305-8565, Japan*

(Received 11 March 2021; revised 30 May 2021; accepted 15 July 2021; published 4 August 2021)

We investigated microscopic lattice states in the donor-acceptor ionic Mott insulator, tetrathiafulvalene-bromanil (TTF-BA), by ^{79}Br-nuclear quadrupole resonance (NQR) spectroscopy to explore cross-correlated fluctuations between spin, charge, and the lattice. A ferroelectric transition with lattice dimerization is captured by a NQR line splitting with the critical exponent β of 0.40 ± 0.03, close to the β value in the three-dimensional Ising universality class, 0.33, and a peak formation in the spin-lattice relaxation rate T_1^{-1} at the transition temperature T_c, of 53 K. Notably, T_1^{-1} does not obey the conventional T^2 law expected for the Raman process of phonons even far above T_c, indicating the emergence of extraordinary lattice fluctuations. They are very probably associated with polar fluctuations in the paraelectric and paramagnetic phase of TTF-BA and explain the anomalously suppressed paramagnetic spin susceptibility prior to the nonmagnetic ferroelectric order as observed by Sunami *et al.* [Phys. Rev. Research **2**, 043333 (2020)].

DOI: 10.1103/PhysRevB.104.L081102

Magnetoelectric cross coupling leads to the control of electric polarizations and magnetic orders by nonconjugate fields in multiferroics [1,2]. One-dimensional (1D) donor-acceptor ionic spin chain is a promising system for giving rise to spin-singlet driven ferroelectricity because an electric polarization is induced by a symmetry-breaking lattice dimerization with spin singlet [3,4]. The organic charge-transfer complex tetrathiafulvalene-bromanil (TTF-BA) is composed of 1D mixed stacks of donor molecules, TTF, and acceptor molecules, BA [Figs. 1(a) and 1(b)] and is in a highly ionic state ($\mathrm{TTF}^{+\rho}$-$\mathrm{BA}^{-\rho}$ with $\rho \sim 0.95$) due to the charge transfer from TTF to BA molecules [5]. TTF-BA is in the paramagnetic and paraelectric state with a spin $1/2$ on each molecule in the uniform 1D ionic chains at room temperature and exhibits a nonmagnetic dimerization (spin-Peierls) transition accompanied by ferroelectricity at $T_c = 53$ K [5–7]. These behaviors are quite different from those of the analogous material tetrathiafulvalene-chloranil (TTF-CA), showing a neutral-ionic (NI) transition from a neutral phase ($\rho \sim 0.3$) to a ferroelectric ionic phase ($\rho \sim 0.6 - 0.7$) at 81 K under ambient pressure [8,9].

It was reported that ferroelectricity near T_c is suppressed by applying a pulsed magnetic field of $\sim$50 T, which suggests that the ferroelectricity is coupled to the spin-singlet formation in TTF-BA [6]. On the other hand, a ^{1}H-nuclear magnetic resonance (NMR) study reveals that, in the paramagnetic phase above T_c, the spin susceptibility does not obey the Bonner-Fisher curve expected in 1D Heisenberg spin systems, and is substantially reduced from the values of the Bonner-Fisher model in a wide temperature range below ambient temperature [10]. It is proposed that this suppression of the susceptibility is driven by polar fluctuations coupled with lattice dimerization inherent in the ionic spin-chain system [10]; however, the nature of lattice states has not been explored yet.

In the present study, we aim to unveil the microscopic lattice states of TTF-BA potentially hosting the cross-correlated fluctuations between spin, charge, and lattice by ^{79}Br-nuclear quadrupole resonance (NQR) spectroscopy, which probes the static and dynamical properties of lattice. We found prominent lattice fluctuations, which are not explainable by either conventional phonons or critical slowing down prior to the ferroelectric order in TTF-BA.

We performed ^{79,81}Br-NQR (nuclear spin $I = 3/2$) measurements on the polycrystalline sample of TTF-BA, in which there are four crystallographically nonequivalent Br sites in the paraelectric state as shown in Fig. 1(b). We employed the spin-echo pulse sequence to obtain NQR signals. The spin-lattice relaxation rate T_1^{-1} was determined by fitting the single exponential function to the relaxation curve of the nuclear magnetization obtained using the standard saturation recovery method.

At room temperature, we observed two sets of four spectra in the frequency ranges of 270–304 MHz and 231–240 MHz [labelled by #1 to #8 from the lowest-frequency peak as shown in Fig. 1(c)]. Br nuclei have two stable isotopes, ^{79}Br ($I = 3/2$, natural abundance $= 50.7\%$, quadrupolar moment $^{79}Q = 0.331\times10^{-24}$ cm^2) and ^{81}Br ($I = 3/2$, natural abundance $= 49.3\%$, quadrupolar moment $^{81}Q = 0.276\times10^{-24}$ cm^2) [11]. The NQR frequency is proportional to both of the electric-field gradient (EFG) at the nuclear position and the nuclear quadrupolar moment. Therefore, each of the four

---

[*] sunami@mdf2.t.u-tokyo.ac.jp

[†] kanoda@ap.t.u-tokyo.ac.jp

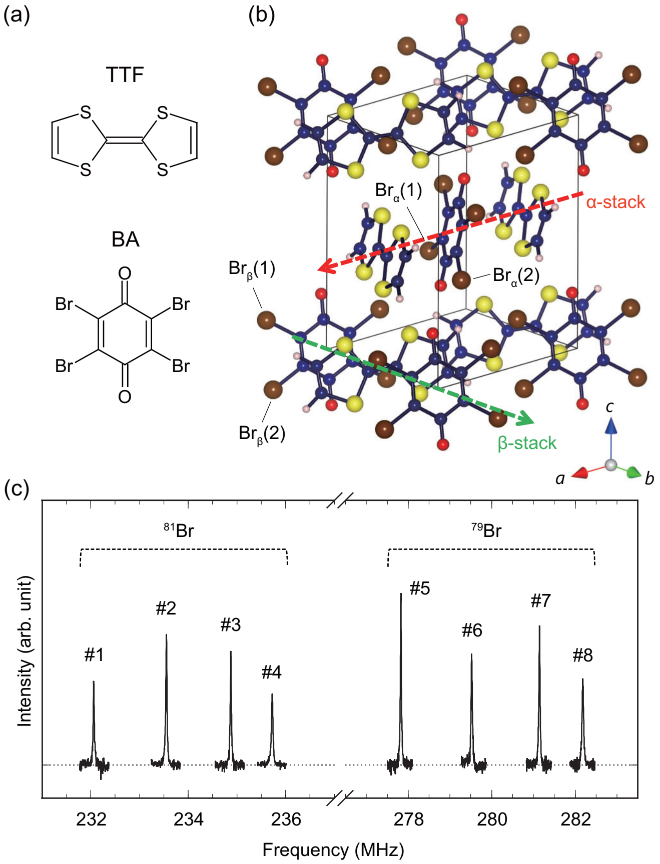

FIG. 1. (a) Molecular structures of TTF and BA. (b) Crystal structure of TTF-BA [7]. (c) ^{79,81}Br-NQR spectra in TTF-BA at room temperature.

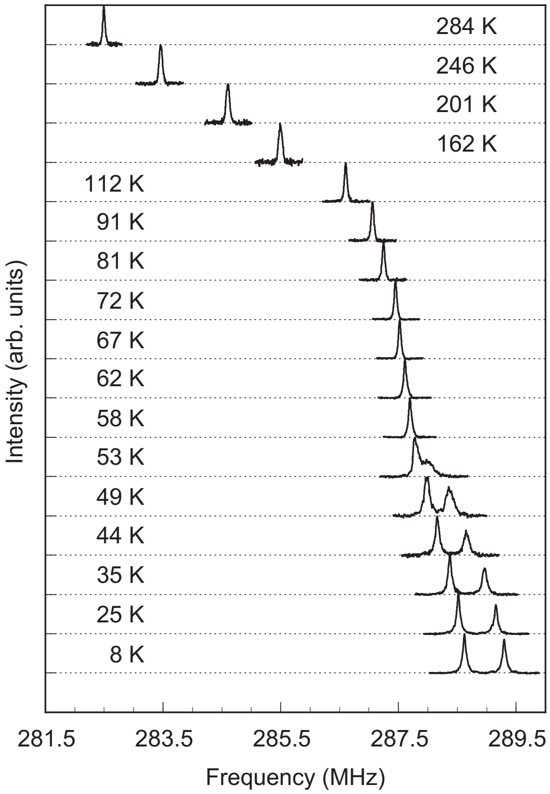

FIG. 2. Temperature variation of ^{79}Br-NQR spectra (line #8) in TTF-BA.

inequivalent sites gives two (^{79}Br and ^{81}Br) NQR lines with the resonance-frequency ratio $^{79}\nu\,/\,^{81}\nu$, equal to $^{79}Q\,/\,^{81}Q = 1.199$. Actually, the observed frequencies of eight spectra, $\nu(1)$–$\nu(8)$, give $\nu(5)/\nu(1) \sim \nu(6)/\nu(2) \sim \nu(7)/\nu(3) \sim \nu(8)/\nu(4) \sim 1.197$; thus, the lines of $\nu(5)$–$\nu(8)$ and $\nu(1)$–$\nu(4)$ are assigned to the ^{79}Br and ^{81}Br NQR lines, respectively. In what follows, we present the temperature profile of the highest-frequency peak (line #8) because all of the lines behave similarly.

Upon cooling, the peak position is shifted to higher frequencies [Figs. 2 and 3(a)], which is well understandable in terms of the thermal-averaging effect of EFG [12–18]. The spectrum splits into two lines at T_c of 53 K, indicative of the loss of inversion center on a BA molecule due to the symmetry-breaking ferroelectric transition [6,7]. The line splitting width Δ_{split} plotted in Fig. 3(b) sharply increases just below T_c, consistent with the continuous phase transition [5,6,10]. The Δ_{split} characterizes the degree of dimerization. Supposing that ν_Q^R and ν_Q^L are the ν_Q values of the two ^{79}Br sites that split upon the ferroelectric transition and Δd is the coordinate characterizing the molecular displacement, $\nu_Q^R(\Delta d)$ and $\nu_Q^L(\Delta d)$ should be analytic functions of Δd without any singularity and the relation of $\nu_Q^R(\Delta d) = \nu_Q^L(-\Delta d)$ should hold, considering the symmetry of the displacement. Thus, $\nu_Q^R(\Delta d)$ and $\nu_Q^L(\Delta d)$ are expanded near $\Delta d = 0$ as $\nu_Q^R(\Delta d) = \nu_{\Delta d=0} + p\Delta d + q\Delta d^2$ and $\nu_Q^L(\Delta d) = \nu_{\Delta d=0} - p\Delta d + q\Delta d^2$, where p and q are coefficients in the expansion. Then, $\Delta_{\text{split}} = |\nu_Q^R - \nu_Q^L| = 2|p||\Delta d|$, which is proportional to the electric polarization, the order parameter of ferroelectricity. Its critical behavior is described by $\Delta_{\text{split}} \propto t^\beta$ with the critical exponent β and the reduced temperature $t = |T - T_c|/T_c$. Fitting the form to the data in $0.02 < t < 0.2$ yields $\beta = 0.40 \pm 0.03$ [Fig. 3(b)], which is close to the β values for the three-dimensional (3D) universality class of interacting spins ($\beta = 0.33$, 0.35, and 0.36 for Ising, XY, and Heisenberg spins, respectively) [19]. This is consistent with the view that the present system of 3D ferroelectric with the Ising-like anisotropic electric polarization is expected to be mapped to the 3D Ising model as observed in the different organic ferroelectric [20].

Besides the splitting, the ν_Q value itself is additionally influenced by the ferroelectric dimerization transition. As shown in Fig. 3(a), upon cooling from room temperature, ν_Q increases and, below T_c, the averaged value of ν_Q, ν_Q^{ave} shows a further rise with a kink at T_c. The smooth increase in ν_Q below room temperature originates from the thermal-averaging effect of EFG [12,13] whereas the additional increase starting at T_c is due to an EFG increase caused by the dimerization transition. It is likely due to the intramolecular charge density redistribution and a change in ρ possibly caused by the dimerization-enhanced hybridization between the highest occupied molecular orbital (HOMO) of TTF and the lowest unoccupied molecular orbital (LUMO) of BA although ρ is not the order parameter of the ferroelectric (dimerization)

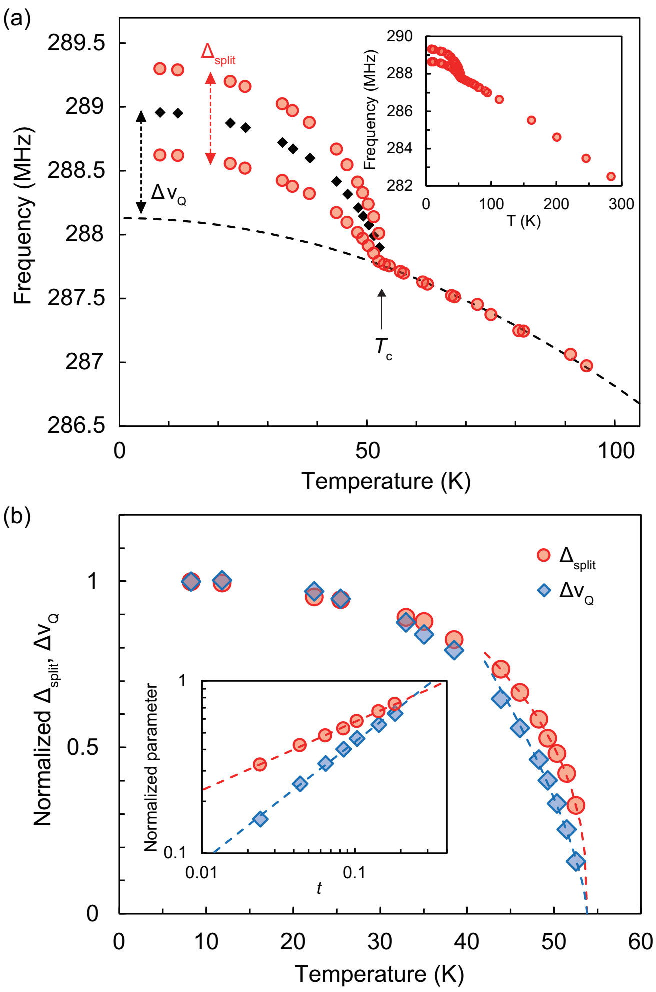

FIG. 3. (a) Temperature profile of the peak frequencies of ^{79}Br -NQR lines (line #8) in TTF-BA (red circles). The averaged values below T_c are plotted by black diamonds. The broken line is the fitting curve with the Koukoulas function, $\nu_Q = \nu_0 \exp(-aT^2)$ [13], to the data for $T_c < T < 100$ K. Inset: Plot of the peak frequency at the entire temperature range below 300 K. (b) The line split width Δ_{split} (red circles) and the frequency shift $\Delta\nu_Q$ (blue diamonds) are plotted (see text for details). These values are normalized to the lowest-temperature values, respectively. The broken lines are fits of the forms of t^β with the critical exponent β and the reduced temperature $t = |T - T_c|/T_c$ to the experimental Δ_{split} and $\Delta\nu_Q$ values for $0.02 < t < 0.2$, respectively. Inset: Log plots of normalized Δ_{split} and $\Delta\nu_Q$ vs. t.

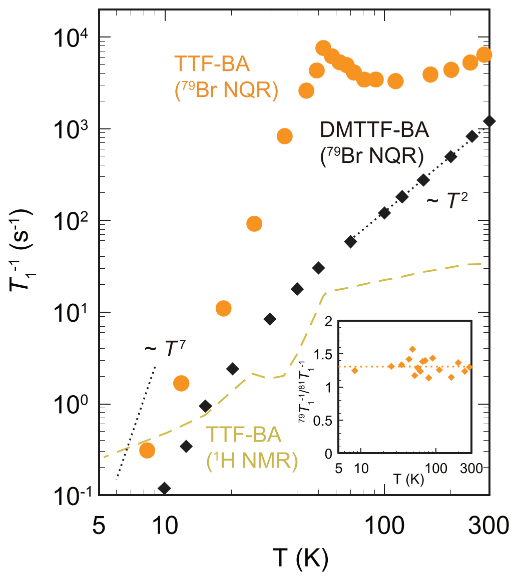

FIG. 4. Temperature dependence of the ^{79}Br -NQR spin-lattice relaxation rate T_1^{-1} in TTF-BA (line #8, orange circles) and DMTTF-BA (black diamonds) reported in Ref. [23], and ^{1}H-NMR T_1^{-1} in TTF-BA (broken yellow line) reported in Ref. [10]. The dotted black lines represent the T^2 and T^7 laws. Inset: Plot of isotope ratio of ^{79}Br and ^{81}Br -NQR relaxation rates $^{79}T_1^{-1}\,/\,^{81}T_1^{-1}$.

transition. Indeed, it was proposed that ρ is backflowed by the dimerization in the ionic phase of the analogous material TTF-CA [17,21]. It is known that the temperature variation of ν_Q due to the thermal-averaging effect of EFG is well described by the empirical formula $\nu_Q = \nu_0 \exp(-aT^2)$ [13]. We fit this form to the ν_Q values in $T_c < T < 100$ K to extrapolate the fitting curve at lower temperatures; the deviation of ν_Q^{ave} from the fitting curve $\Delta\nu_Q$ below T_c is plotted as a function of temperature in Fig. 3(b) and its inset, which show that $\Delta\nu_Q$ is well described by the form of $\Delta\nu_Q \propto t^{\beta'}$ with $\beta' = 0.69 \pm 0.02$. This value is larger than $\beta = 0.40 \pm 0.03$ for Δ_{split}. As Δ_{split} is approximately proportional to the molecular displacement Δd, it turns out that $\Delta\nu_Q \propto \Delta d^{1.7\pm0.1}$. This exponent indicates that $\Delta\nu_Q$ is a higher-order correction to ν_Q with respect to Δd. Using the above formulas, $\Delta\nu_Q$ is given by $\Delta\nu_Q = (\nu_Q^R + \nu_Q^L)/2 - \nu_{\Delta d=0} = q\Delta d^2$, which may explain the observed exponent of 1.7 ± 0.1.

The temperature dependence of spin-lattice relaxation rate T_1^{-1} of line #8 is shown in Fig. 4. T_1^{-1} moderately decreases with temperature down to ~100 K and, in turn, increases on approaching T_c, followed by a sharp peak at T_c, which is reminiscent of the critical behavior typical of the second-order transition. The behavior is different from that of ^{1}H-NMR relaxation rate (Fig. 4) probing the magnetic relaxation owing to no quadrupole moment [10]. This means that the ^{79}Br -NQR T_1^{-1} mainly probes lattice fluctuations through quadrupole interaction instead of magnetic fluctuations through hyperfine interaction. Indeed, the isotope ratio of ^{79}Br and ^{81}Br -NQR relaxation rates $^{79}T_1^{-1}\,/\,^{81}T_1^{-1}$ is 1.31 ± 0.11 independent of temperature [inset of Fig. 4], which is near the squared isotope ratio of quadrupole moments, $(^{79}Q\,/\,^{81}Q)^2 = 1.44$ for quadrupole relaxation rather than that of gyromagnetic ratio, $(^{79}\gamma\,/\,^{81}\gamma)^2 = 0.86$ for magnetic relaxation. In general, the phonon-induced NQR T_1^{-1} should obey the T^2 law due to the two-phonon Raman process for $T > \Theta$, where Θ is the Debye temperature [22]. Actually, an analogous but ferroelectricity-free material, DMTTF-BA with $\Theta = 80$ K, shows ^{79}Br -NQR T_1^{-1} that follows the T^2 law above 100 K, as shown in Fig. 4 [23]. Below ~100 K, the decrease in T_1^{-1} becomes steeper and approaches the T^7 law expected for $T \ll \Theta$ [22]. T_1^{-1} in TTF-BA rapidly decreases with temperature below T_c and approaches the values in DMTTF-BA at low temperatures, say, below 20 K, where the critical enhancement is expected to be considerably diminished. However, T_1^{-1} in the paramagnetic phase does not follow the T^2 law and the absolute values are largely enhanced from those of DMTTF-BA. Although the Θ value of TTF-BA is not known, it is presumably similar to that of DMTTF-BA, considering the common columnar structures; for reference, Θ in TTF-CA is 84 K in the neutral phase and 90 K in the ionic phase [24]. In addition, the nearly the same ν_{Q} values at room temperature between TTF-BA (282 MHz) and DMTTF-BA (297 MHz [23]) as well as the similar atomic and molecular surroundings of the Br nuclei suggest that the quadrupolar coupling is not so different between the two systems. These results strongly suggest that the extraordinarily enhanced lattice fluctuations distinct from the conventional phonons are developed in the paramagnetic phase of TTF-BA. Usually, the enhancement of T_1^{-1} due to the critical slowing down of lattice fluctuations toward the phase transition is observable below $\sim 2T_{\mathrm{c}}$, and, for $T > \sim 2T_{\mathrm{c}}$, where the critical fluctuations almost vanish and the relaxation is caused by the conventional phonons, T_1^{-1} is proportional to T^2 [16,18]. The present enhancement of T_1^{-1} observed around room temperature ($\sim$ 5–6T_{c}) is obviously out of the conventional behavior.

What is the origin of the extraordinary lattice fluctuations in the paramagnetic and paraelectric phase of TTF-BA? In the ionic spin-chain system, the local donor-acceptor pairing is associated with the polar fluctuations due to the displacement of cations and anions, evoking a view that these polar fluctuations promote the local dimer fluctuations even above T_{c} and cause the precursory spin-singlet formation even in the paramagnetic phase, consistent with the suppression of the spin susceptibility reported in Ref. [10]. The local lattice dimerization can be detected by infrared (IR) spectroscopy; the a_g mode of BA molecule is activated when the inversion center on the BA molecule is lost due to the dimerization. Remarkably, the a_g mode keeps being activated even up to $\sim$120 K far above T_{c} [5,6]; however, it fades out above $\sim$120 K. The apparent discrepancy between the NMR/NQR and IR results at high temperatures may stem from different sensitivities of magnetism (singlet formation) and molecular vibration (a_g mode activation) to the dimerization. Another possible manifestation of distinct lattice dynamics above T_{c} is the frequency-dependent dielectric constants in the paraelectric phase, which is increased upon lowering frequency in the range of 0.1–100 kHz [25]. Such a behavior is often observed in the symmetry-broken phase, where fluctuations of ferroelectric domain walls with the characteristic timescale of $\sim$kHz leads to the dielectric dispersion [25,26]. However, in TTF-BA, the prominent frequency dependence of dielectric constants is detected in the paraelectric phase with the uniform 1D chains. This may suggest a case in which dimer singlets associated with the donor-acceptor pairs fluctuate in the form of domains containing several pairs in the paraelectric phase. Considering the spin exchange coupling of $\sim$140 K in TTF-BA [10], the anomalous lattice (dimer) fluctuations persistent up to room temperature are most likely to be not only of spin origin but also assisted by the formation of polarized domains.

In conclusion, ^{79}Br -NQR spectroscopy revealed that the donor-acceptor ionic spin-chain system TTF-BA hosts extraordinary lattice fluctuations prior to the nonmagnetic ferroelectric order as indicated by the relaxation-rate behavior qualitatively different from the phonon-dominated T^2 law in the paramagnetic phase. This points to anomalously enhanced lattice fluctuations possibly coupled with the polar fluctuations inherent in the ionic spin-chain system. The spectral splitting and the peak formation of spin-lattice relaxation rate evidence the ferroelectric transition at 53 K with the critical exponent β of the order parameter 0.40 ± 0.03, which is close to the exponent of the 3D Ising universality class 0.33. The present results lend supports to the emergence of distinct cross-correlated fluctuations between spin, charge, and lattice in a charge-transfer organic complex TTF-BA.

This work was supported by the JSPS Grant-in-Aids for Scientific Research (Grants No. JP18H05225, No. JP19H01846, No. JP20K20894, and No. JP20KK0060).

[1] T. Kimura, T. Goto, H. Shintani, K. Ishizaka, T. Arima, and Y. Tokura, Nature (London) **426**, 55 (2003).

[2] N. Hur, S. Park, P. A. Sharma, J. S. Ahn, S. Guha, and S. W. Cheong, Nature (London) **429**, 392 (2004).

[3] R. E. Peierls, *Quantum Theory of Solids* (Clarendon Press, New York, 1955).

[4] M. C. Cross and D. S. Fisher, Phys. Rev. B **19**, 402 (1979).

[5] A. Girlando, C. Pecile, and J. B. Torrance, Solid State Commun. **54**, 753 (1985).

[6] F. Kagawa, S. Horiuchi, M. Tokunaga, J. Fujioka, and Y. Tokura, Nat. Phys. **6**, 169 (2010).

[7] P. García, S. Dahaoui, P. Fertey, E. Wenger, and C. Lecomte, Phys. Rev. B **72**, 104115 (2005).

[8] J. B. Torrance, J. E. Vazquez, J. J. Mayerle, and V. Y. Lee, Phys. Rev. Lett. **46**, 253 (1981).

[9] J. B. Torrance, A. Girlando, J. J. Mayerle, J. I. Crowley, V. Y. Lee, P. Batail, and S. J. LaPlaca, Phys. Rev. Lett. **47**, 1747 (1981).

[10] K. Sunami, Y. Sakai, R. Takehara, H. Adachi, K. Miyagawa, S. Horiuchi, and K. Kanoda, Phys. Rev. Res. **2**, 043333 (2020).

[11] P. Raghavan, At. Data Nucl. Data Tables **42**, 189 (1989).

[12] H. Bayer, Z. Phys. **130**, 227 (1951).

[13] A. A. Koukoulas and M. A. Whitehead, Chem. Phys. Lett. **167**, 379 (1990).

[14] M. Gourdji, L. Guibé, A. Péneau, J. Gallier, B. Toudic, and H. Cailleau, Solid State Commun. **77**, 609 (1991).

[15] J. Gallier, B. Toudic, Y. Delugeard, H. Cailleau, M. Gourdji, A. Péneau, and L. Guibé, Phys. Rev. B **47**, 11688 (1993).

[16] F. Iwase, K. Miyagawa, S. Fujiyama, K. Kanoda, S. Horiuchi, and Y. Tokura, J. Phys. Soc. Jpn. **76**, 073701 (2007).

[17] R. Takehara, K. Sunami, F. Iwase, M. Hosoda, K. Miyagawa, T. Miyamoto, H. Okamoto, and K. Kanoda, Phys. Rev. B **98**, 054103 (2018).

[18] K. Sunami, F. Iwase, K. Miyagawa, S. Horiuchi, K. Kobayashi, R. Kumai, and K. Kanoda, Phys. Rev. B **99**, 125133 (2019).

[19] J. C. Le Guillou and J. Zinn-Justin, Phys. Rev. B **21**, 3976 (1980).

[20] T. Asaji, K. Gotoh, and J. Watanabe, J. Mol. Struct. **791**, 89 (2006).

[21] N. Nagaosa, J. Phys. Soc. Jpn. **55**, 2754 (1986).

[22] A. Abragam, *The Principles of Nuclear Magnetism* (Oxford University Press, Oxford, 1961).

[23] F. Iwase, K. Miyagawa, K. Kanoda, S. Horiuchi, and Y. Tokura, J. Phys. Soc. Jpn. **79**, 043709 (2010).

[24] T. Kawamura, Y. Miyazaki, and M. Sorai, Chem. Phys. Lett. **273**, 435 (1997).

[25] Y. Tokura, S. Koshihara, Y. Iwasa, H. Okamoto, T. Komatsu, T. Koda, N. Iwasawa, and G. Saito, Phys. Rev. Lett. **63**, 2405 (1989).

[26] F. Kagawa, S. Horiuchi, H. Matsui, R. Kumai, Y. Onose, T. Hasegawa, and Y. Tokura, Phys. Rev. Lett. **104**, 227602 (2010).